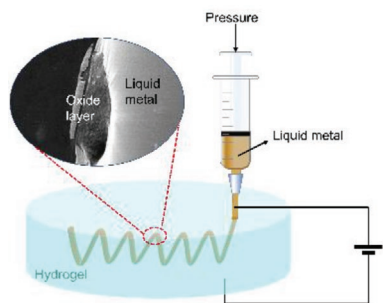


RESEARCH ARTICLES

X. Wang, L. Li, X. Yang,
H. Wang, J. Guo, Y. Wang, X. Chen,
L. Hu^{*}.....2100228

Electrically Induced Wire-Forming 3D Printing Technology of Gallium-Based Low Melting Point Metals



A universal electrically induced wire-forming 3D suspending printing technology of gallium-based liquid metal is proposed. Taken galinstan as an example, the printing conditions, including the viscosity of hydrogel, voltage, calcium chloride concentration, and velocity are explored to optimize the process. And the printed galinstan is characterized by scanning electron microscope, energy dispersive spectrometer, and X-ray photoelectron spectrometer.



Electrically Induced Wire-Forming 3D Printing Technology of Gallium-Based Low Melting Point Metals

Xinpeng Wang, Liangtao Li, Xiawei Yang, Hongzhang Wang, Jiarui Guo, Yang Wang, Xuanqi Chen, and Liang Hu*

Low-melting point metals and alloys, as emerging 3D printing ink, have attracted more and more attention especially for flexible or intelligent conductors and electronics. However, achieving 3D continuity of liquid metal structures or patterns using a common method is still challenging and worth pursuing. In this study, a generalized method is proposed for 3D printing structures made of low melting gallium-based alloys with diverse melting points, which should greatly expand their applications. The mechanism for shaping liquid metal inks relies on the combination actions between electrocapillarity and oxidation, which significantly reduces the high surface tension as well provides solid frame for the inner liquid metals. Taken galinstan as an example, the printing conditions, including the viscosity of hydrogel, positive voltage (0–15 V), calcium chloride concentration, and velocity (the movement speed of the printing head) are explored to optimize the process. The printed galinstan is characterized to observe the morphology and elemental analysis of the surface oxide layer. During the process, the chemical reagents are all safe and non-toxic, which is in line with the green product requirements. This printing method shall have broad application prospect in flexible electronics, biosensors, biomedical engineering, contrast agent *in vivo*, and other fields.

1. Introduction

3D printing technology is also known as additive manufacturing (AM) technology,^[1–4] which is a layer-by-layer fabrication of objects. The categories of 3D printing materials or inks mainly include polymer materials, metal materials, and ceramic materials. Among these materials, metal 3D printing is currently widely used in the aerospace industries, consumer electronics,^[5–7] biomedical,^[8–11] construction,^[12] etc. to produce high-value end-use parts, which are highly customized or produced in small quantities. However, traditional metals have high melting temperature, which requires high energy consumption for further printing process. Besides, the solid-state of those metals is not compatible with most soft materials such as elastomer, which limits their applications in flexible electronics.

Recently, gallium-based liquid metal (GLM), as direct writing of electronics, based on alloy and metal (DREAM)

ink,^[13–17] owns not only high electrical conductivity and high thermal conductivity in the fluid materials but also has good rheological property, safety, and biocompatibility, which has been greatly expanded in more and more application fields.^[18–21] Meanwhile, compared to the traditional metal inks, liquid metal has many advantages such as moderate processing temperature, simple preparation, no post-treatment processes. Recently, due to the unique properties mentioned above, liquid metal has attracted wide attention from researches in 3D printing and wearable devices.^[5,10,19,22–24] Among that, Yu et al. proposed a suspension 3D printing of liquid metal into hydrogel.^[25] It is illustrated that this suspension printing method had potential application in constructing 3D macro-structure and stereo electronic systems. However, in this work due to the high surface tension, the liquid metal still present spherical droplets in the hydrogel, which greatly limits its resolution and shaping styles for more potential applications. To overcome the high surface tension of GLMs, many methods such as surface modification, physical doping, and electric induction have been presented.^[16,26] Among those methods, electric induction has the characteristic of not changing the nature of liquid metal itself (viz. electrical conductivity) so

X. Wang, J. Guo, Y. Wang, X. Chen, L. Hu
Beijing Advanced Innovation Center for Biomedical Engineering
Institute of Nanotechnology for Single Cell Analysis (INSCA)
Beihang University
Beijing 100191, P. R. China
E-mail: cnhuliang@buaa.edu.cn

X. Wang, L. Li, J. Guo, Y. Wang, X. Chen, L. Hu
School of Biological Science and Medical Engineering
Beihang University
Beijing 100191, P. R. China

X. Yang
State Key Laboratory of Solidification Processing
Shaanxi Key Laboratory of Friction Welding Technologies
Northwestern Polytechnical University
Xi'an, Shaanxi 710072, P. R. China

H. Wang
Department of Biomedical Engineering
School of Medicine
Tsinghua University
Beijing 100084, P. R. China

 The ORCID identification number(s) for the author(s) of this article can be found under <https://doi.org/10.1002/admt.202100228>.

DOI: 10.1002/admt.202100228

that liquid metal could be extended to many applications by controlling the electrical conditions. Initially, Dickey's group showed that the interfacial tension in an alkaline medium can be reduced substantially by electrocapillarity and oxidation.^[26] And it was shown that wire formation and 2D deposition are possible via this technique,^[27] while Wang et al. showed that liquid metal could penetrate meshes and other porous materials by application of a positive voltage.^[21] Interestingly, Kalantar-Zadeh's group presented that the direct synthesis and expulsion of metals from alloys could be realized electrochemically by applying a polarizing voltage signal to liquid alloys. The signal induces an abrupt interfacial perturbation at the Ga-based liquid alloy surface and results in an unrestrained discharge of minority elements, such as Sn, In, and Zn, from the liquid alloy,^[28] which is called dealloying. Moreover, combined with suspension printing, in our previous work, we have overcome this limitation by developing an electrochemically enabled embedded 3D printing (3e-3DP) technology to print wirelike pure gallium 3D structures.^[29] The combination actions between electrocapillarity and formation of gallium oxide layer play a vital role in the wirelike shaping by significantly reducing the surface tension^[26,27,29] and providing mechanical support and solid frame for inner liquid parts.

To further develop this printing technology as well as to broaden the potential applications of low melting point alloys, in this study, we explore the 3D printing of several gallium-based alloys with diverse melting points. This result suggests most gallium-based alloys can be applied in this 3e-3DP technology due to the obvious formation of gallium oxide with positive voltage applied. Moreover, taking galinstan ($\text{Ga}_{68.5}\text{In}_{21.5}\text{Sn}_{10}$) as an example, we explore and optimize the printing conditions including the viscosity of hydrogel, positive voltage, calcium chloride concentration, and velocity (the movement speed of the printing head). During the process, the chemical reagents are all safe and non-toxic, which is in line with the green product requirements. This study will open more opportunities for gallium-based low melting points alloys for their application prospect in flexible electronics, biosensors, biomedical engineering, contrast agent in vivo, injection electronics, and other fields.

2. Results and Discussion

Based on our previous study, the gallium oxide formation is vital in this wirelike shaping with positive voltage applied, which suggests gallium elements may be the key for the metal alloys in this 3e-3DP method.^[29] To explore the possibility of 3e-3DP for low melting points alloys, we tested several metal alloys including gallium-based alloys and bismuth-based alloys. These alloys, including Ga, $\text{Ga}_{75.5}\text{In}_{24.5}$, $\text{Ga}_{68.5}\text{In}_{21.5}\text{Sn}_{10}$, $\text{Ga}_{51.6}\text{In}_{48.4}$, $\text{Ga}_{44.2}\text{In}_{55.8}$, $\text{Ga}_{52.1}\text{Bi}_{15.1}\text{In}_{23.4}\text{Sn}_{9.4}$, $\text{Ga}_{43.5}\text{Bi}_{17.9}\text{In}_{27.6}\text{Sn}_{11}$, $\text{Bi}_{31.6}\text{In}_{48.8}\text{Sn}_{19.6}$ were separately added into a beaker and were heated to corresponding melting points related to alloy compositions.^[30-34] Then, the metal droplets were put into a neutral solution (here is CaCl_2). The positive electrode of the power connects the metal, the negative electrode is placed in the solution, the voltage ranges from 0–15 V. Based on movie 1–8, we measured the change of LM diameter

under different voltages. As shown in the relationship between $\Delta d/d_0$ and voltage (Figure 1a,b), we found that gallium-based alloys (Ga , $\text{Ga}_{75.5}\text{In}_{24.5}$, $\text{Ga}_{68.5}\text{In}_{21.5}\text{Sn}_{10}$, $\text{Ga}_{51.6}\text{In}_{48.4}$) could be deformed at 0–15 V and not produce too many impurities (such as bubbles and black layer in movie). We could infer from our previous printing experiments that the percent content of gallium in the alloys should be $\geq 50\%$ to have chance to print continuous wire structure in the gelatin hydrogel and not produce too many impurities (such as bubbles and black layer). That is because the mechanism of this electrochemical printing method depends on the reduced surface tension caused by oxidation and electrocapillarity.^[26,27,35] With the formation of the oxide layer, the printed liquid metal could form core-shell structure and liquid metal (core) flows in the oxide layer (shell) to form the continuous liquid metal wires. The results also revealed that $\text{Ga}_{52.1}\text{Bi}_{15.1}\text{In}_{23.4}\text{Sn}_{9.4}$, $\text{Ga}_{43.5}\text{Bi}_{17.9}\text{In}_{27.6}\text{Sn}_{11}$, $\text{Bi}_{31.6}\text{In}_{48.8}\text{Sn}_{19.6}$ showed small deformation in a very narrow voltage range. Especially, $\text{Bi}_{31.6}\text{In}_{48.8}\text{Sn}_{19.6}$, without gallium, could not be deformed under 7 V and deformed a little during 7–9 V without obvious black layer. It is consistent with the previous work that bismuth, indium, or tin is a relatively stable element compared with gallium.^[27,32,36] The reason might be that gallium is easy to be oxidized in the electrolyte. With the increasing proportion of gallium, the alloys are easier to form the oxide layer and reduce the surface tension after applied voltage. Notably, even though it is oxidized, from observation, we presume that the oxide may not be able to provide enough surface tension reduction and to support the deformation in this printing method at 0–15 V. As the melting point is raised to around 50 °C (Figure 1c and Figure S1, Supporting Information), some bubbles will be produced and could disturb the printing structure, which could also be seen in the movies. Notably, as the bubbles and black layer will produce and be disrupted when the voltage increases to a certain level, the oxide layer will be destroyed simultaneously, and then the diameter will become smaller rather than larger, such as $\text{Ga}_{43.5}\text{Bi}_{17.9}\text{In}_{27.6}\text{Sn}_{11}$ at 15 V. Thus, Ga/GaIn/GaInSn (the percent content of gallium in the alloys should be $\geq 50\%$) are recommended to be printed using 3e-3DP technology. While bismuth-based alloys could not be suggested to be printed in gel by this method at 0–15 V. To make it more clearly, we used different background color to distinguish the recommended printed metals (red background color) and not printed alloys (green background color) as illustrated in Figure 1c. It could be seen that gallium-based alloys own different melting points, which could be applied in different conditions and be printed into different structures. This will play an important role in a variety of potential applications.

Then, taken galinstan (GaInSn) as an example, the control and optimization of printing conditions are explored. The printing system was shown in Figure 2 schematically, fabricated by three parts, including 3D printing system, voltage stabilizer, and injection pump. The wire-forming printing principle of GaInSn was shown in Figure 3a. It can be seen that the anode was connected with the spring needle (Figure S2, Supporting Information), which will have liquid metal squeezed out. The inner diameter of the spring needle used in the experiments is 0.61 mm. The cathode was inserted into the gelatin hydrogel. It is known that the surface tension of LM is declined when

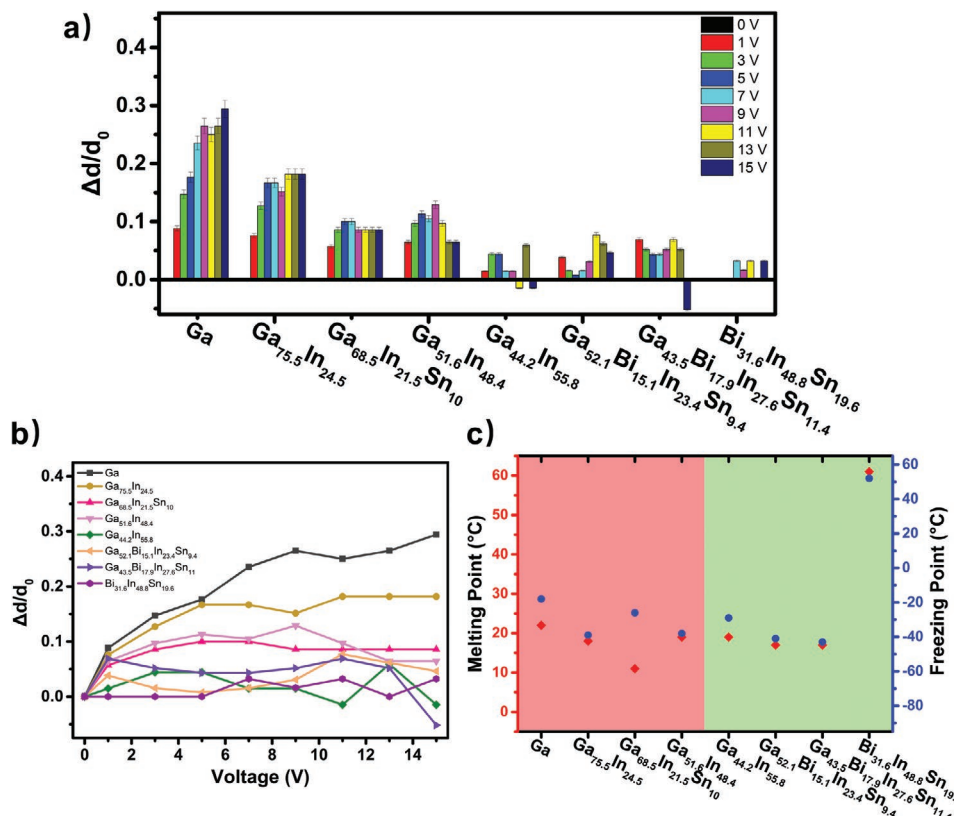


Figure 1. a,b) The diameter change of different liquid metals during 0–15 V. c) Melting point and freezing point of some different gallium-based alloys, including recommended printed metals (red background color) and not recommended printed alloys (green background color).

connected with oxidative electrical potential^[37–39] due to the combination of electrocapillarity and the oxidation. Briefly, the application of an electrical voltage changes the structure of the

electrical double layer (EDL), changing the surface tension. As described in Lippmann's equation, the surface tension of the LM has a square dependence over the gradient of the potential

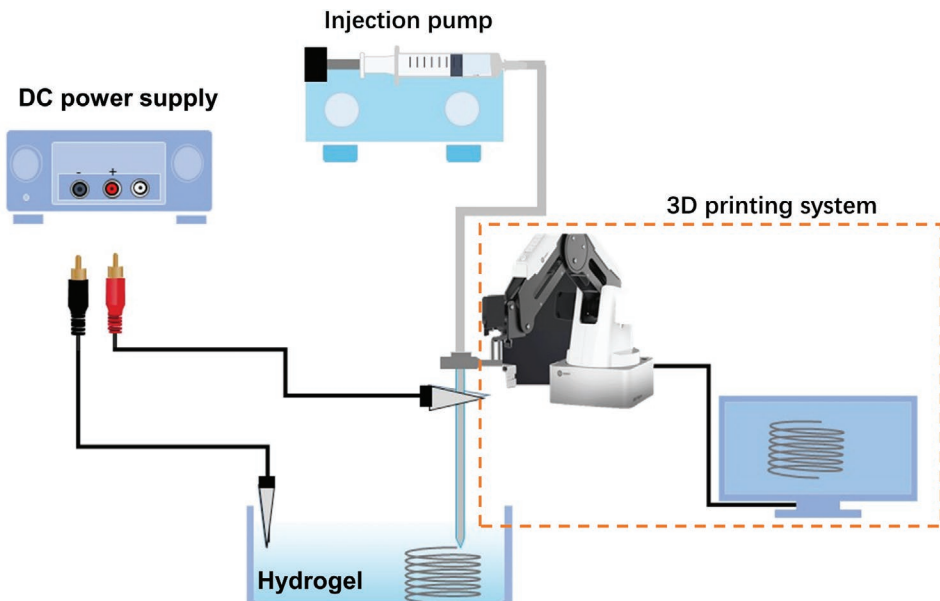


Figure 2. Schematic diagram of electrically induced wire-forming 3D printing system.

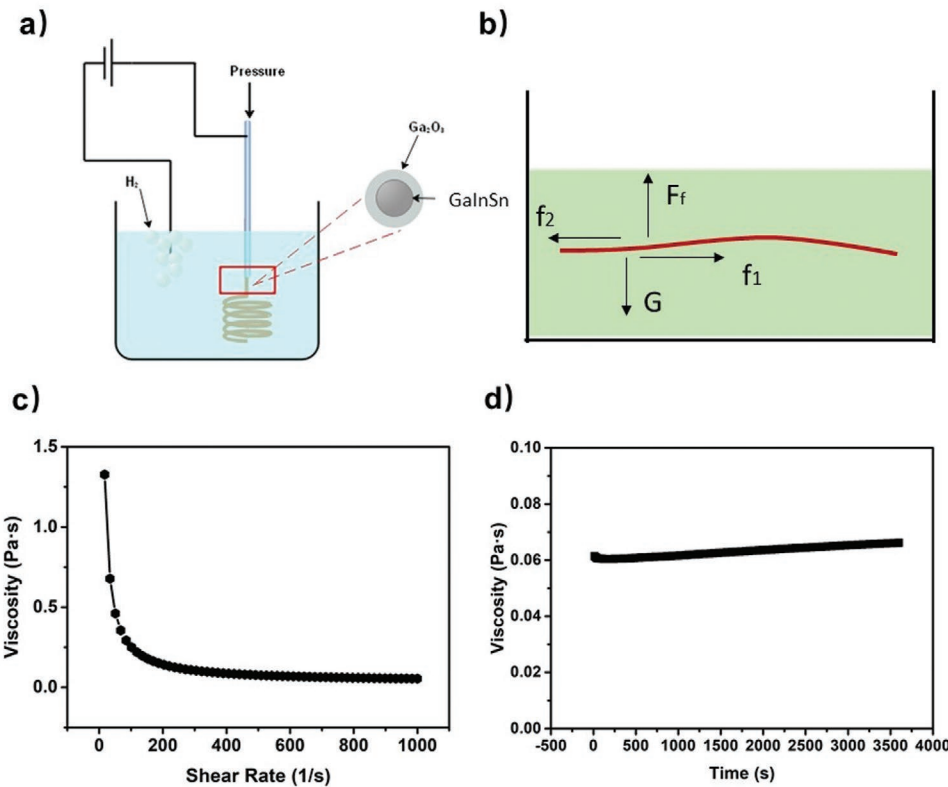


Figure 3. a) The wire-forming printing principle of GaInSn. b) The force analysis of printed LM during the gelatin hydrogel. c,d) The viscosity of the gelatin when it can be used in the printing of GaInSn alloy at different shear rate and steady time, respectively.

(approximately equivalent to the applied external voltage) across the EDL as follows

$$\gamma = \gamma_0 - \frac{1}{2} C (\varphi - \varphi_0)^2 \quad (1)$$

where γ_0 is the maximum surface tension, C is the EDL capacitance per unit area, φ is the EDL potential, and φ_0 is the potential of zero charge. It could be concluded that any applied voltage, either positive or negative, results in the decrease of the surface tension.

The applied positive voltage also results in the formation of the oxide layer on the LM surface, the reactions have happened as follows.



Initially, based on previous research experience, the extruded velocity ($200 \mu\text{L min}^{-1}$) and the concentration of gelatin (5% w/w) were selected in the whole experiments for the printing process. The force was analyzed as shown in Figure 3b. To realize the wire-forming printing in hydrogel, on the one hand, the hydrogel should have the supporting capacity (F_f), which is related to the gravity (G). On the other hand, the resistance of hydrogel (f_1) should keep good balance with the force forward (f_2). Thus, we detected the viscosity of the gelatin when it could be used in the

printing of GaInSn alloy (Figure 3c,d). The result showed that the viscosity should maintain around 0.06 Pa·s (about 3600 s within 5% change at room temperature) at the shear rate of 1000 1/s and the viscosity will increase with the standing time due to further crosslinking. To keep the consistency during experiments, it must be printed as soon as possible. If the viscosity could be maintained stable for longer time, it could be beneficial for printing more complex structures. 3D printing wire structure of GaInSn in gelatin hydrogel is shown in Movie S9, Supporting Information, suggesting the feasibility of this method and indicating the potential value in printing more 3D structures applied in personalized customization field.

To further clarify the wire-forming conditions, we explored the effect of different voltage (1, 3, 5, 7, 9, 11 V), different calcium chloride concentration (20, 40, 60, 80 mM), and different velocity (5, 10, 25, 50, 100 mm s⁻¹). As shown in Figure 4a, the wire-forming velocity increases as the concentration increases. Under 3 V, it is hard to form GaInSn continuous wires in the gel, due to the large surface tension of liquid metal (Figure 4b above). In the voltage range of 3–7 V, with appropriate velocity, the fiber can be formed without black layer (Figure 4b bottom and Figure 4c). Above the condition, it can be seen a black layer will form on the surface of LM during printing (Figure 4d).

Moreover, the factors that affect the diameter of the wire were explored shown in Figure 5a-c, printing voltage, depth, and velocity, respectively. As depicted in Figure 5b, we can conclude that the effect of voltage is negligible. The diameter is measured at different voltages with different states (maybe

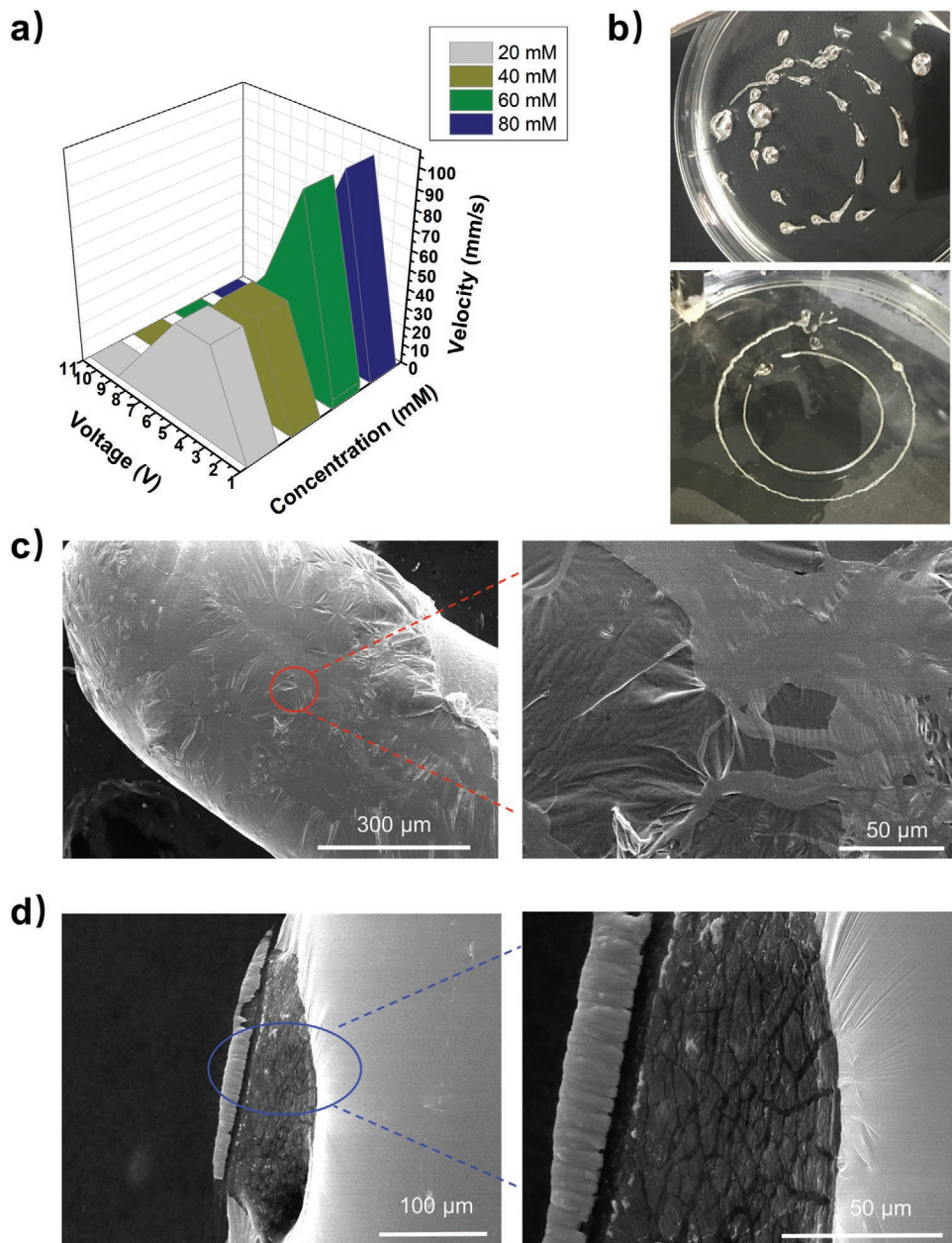


Figure 4. a) The wire-forming conditions with voltage, concentration, velocity. b) The photograph of non-wire (above) and wire-forming (bottom). c,d) SEM graphs of GaInSn with normal oxide layer and black oxide layer, respectively.

discontinuous liquid metal wire) as shown in Figure 4b. The influence of printing depth was investigated. In Figure 5c, we can see that the diameter decreases as the depth increases because of the hydrogel pressure, and then stabilizes. During $10\text{--}40\text{ mm s}^{-1}$ (Figure 5a), with increasing the velocity, the diameter increased. Above 40 mm s^{-1} , the diameter decreased. That is because the liquid metal has trend to accumulate and aggregate into balls at low velocity to make the wire diameter is smaller. At high velocity, as the tension increases, the liquid metal flows out less and the diameter is smaller. Totally, the mean diameter is around $350\text{ }\mu\text{m}$. Through the above exploration, we selected optimized experimental conditions (3 V , 40 mM , 50 mm s^{-1} , 1 mm depth) for subsequent experiments.

To characterize the surface morphology of the formed alloy, scanning electron microscope (SEM) was used. Numerous wrinkles can be seen on the surface at high magnification in Figure 4c and Figure 6a above. Black oxide film formed by high voltage was cracked and porous (Figures 4d and 6a bottom), which showed unstable after standing for a while.

To analyze the elements of the black oxide layer, energy dispersive spectrometer (EDS) and X-ray photoelectron spectrometer (XPS) were used. As shown in Figure 6a, concluded from the EDS result, the content of oxygen is higher in black oxide layer, which is related to the cracked and porous structure containing more oxygen. It could also be seen in Figure S3 and Table S1, Supporting Information, the mapping images

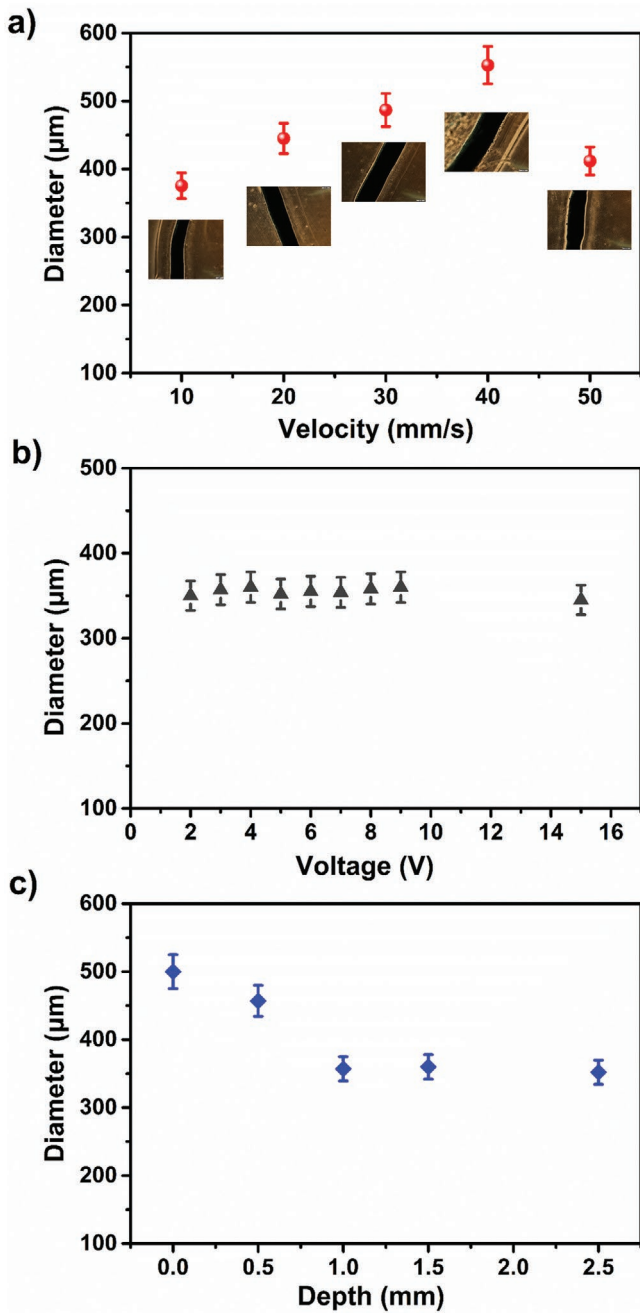


Figure 5. The relationship between diameter and velocity (a), voltage (b), and depth (c).

of EDS and atomic percentage (%) of elements at different voltages show the oxygen content increases as the voltage increases quantificationally, especially after changing into black oxide layer (9 V). This result is consistent with the XPS result. It can be seen from the XPS data (Figure 6b) that the black layer has Mn and Ti, which conforms to our hypothesis. During the experiments, it can be observed that the black layer wasn't stable. We infer that one reason may lie in that the cracked and porous structure is not dense. The other reason may be that the inner metal needs further oxidation with continuous voltage on, then produce a force to destroy the outer

loose layer. Here, to a great extent, the XPS result suggests that the black oxide layer produced at high voltage is attributed to the oxidation of spring needle, which is made of stainless steel. Furthermore, as the black oxide layer is unstable and undesirable for further applications, it is important to control the printing conditions. Moreover, to avoid the oxidation of spring needle, it has been proved that PTFE needles or fluorocarbon needles could be used,^[40] and that the electrode could be replaced by graphite or diamond electrodes. The resistance of liquid metal wire was around $0.1\ \Omega$, and has little change through the printing process, which demonstrates the great potential of this printing method in flexible electronics. More comparison of printing liquid metals wire could be seen in Table S2, Supporting Information. It shows that the printing liquid metal wire by electrochemical extrusion method owns advantage in electrical conductivity and still has many research potentials to explore.

3. Conclusion

In this research, a universal electrically induced embedded wire-forming 3D printing method for low melting point metals is introduced. The mechanism for shaping of liquid metal inks in this work relies on the combination actions between electrocapillarity and formation of gallium oxide layer, which significantly reduces the high surface tension as well provides solid frame for the inner liquid metals. The printing conditions, including the viscosity of gelatin hydrogel, voltage, depth, and velocity were optimized (3 V , 40 mM , 50 mm s^{-1} , 1 mm depth). The mean diameter is around $350\ \mu\text{m}$. During the process, the chemical reagents are all safe and non-toxic, which is in accordance with the green product requirements. Moreover, the surface morphology of LM wire (the resistance is $0.1\ \Omega$) was characterized, and the elements were analyzed, which is beneficial for further exploration. Based on the mechanism of wire-forming, the formation of oxide layer on the surface of liquid metal will promote printing continuously. Compared with several kinds of alloys, the gallium alloys ($\text{Ga}/\text{GaIn}/\text{GaInSn}$) with gallium proportion higher than 50% (w/w) are more likely to be applied in this 3e-3DP method to form continuous wire structures under moderate voltage without producing too many impurities (such as bubbles and black layer). While bismuth-based alloys are not recommended for this method at $0\text{--}15\text{ V}$. Hence, GLMs with appropriate ratio and different melting points could be printed using this method, which could be applied in different environments. This work establishes a novel 3D printing method for low-melting point metals, which shall open more opportunities in metallic fabrication, flexible electronics, and other fields.

4. Experimental Section

Materials and Methods: Gallium-based alloys and bismuth-based alloys, including Ga , $\text{Ga}_{75.5}\text{In}_{24.5}$, $\text{Ga}_{68.5}\text{In}_{21.5}\text{Sn}_{10}$, $\text{Ga}_{51.6}\text{In}_{48.4}\text{I}$, $\text{Ga}_{44.2}\text{In}_{55.8}$, $\text{Ga}_{52.1}\text{Bi}_{15.1}\text{In}_{23.4}\text{Sn}_{9.4}$, $\text{Ga}_{43.5}\text{Bi}_{17.9}\text{In}_{27.6}\text{Sn}_{11}$, $\text{Bi}_{31.6}\text{In}_{48.8}\text{Sn}_{19.6}$, were separately added into a beaker and were heated to corresponding melting points related to different ratios. For example, the experiments were carried out on the eutectic liquid-metal GaInSn alloy (Ga 68.5%,

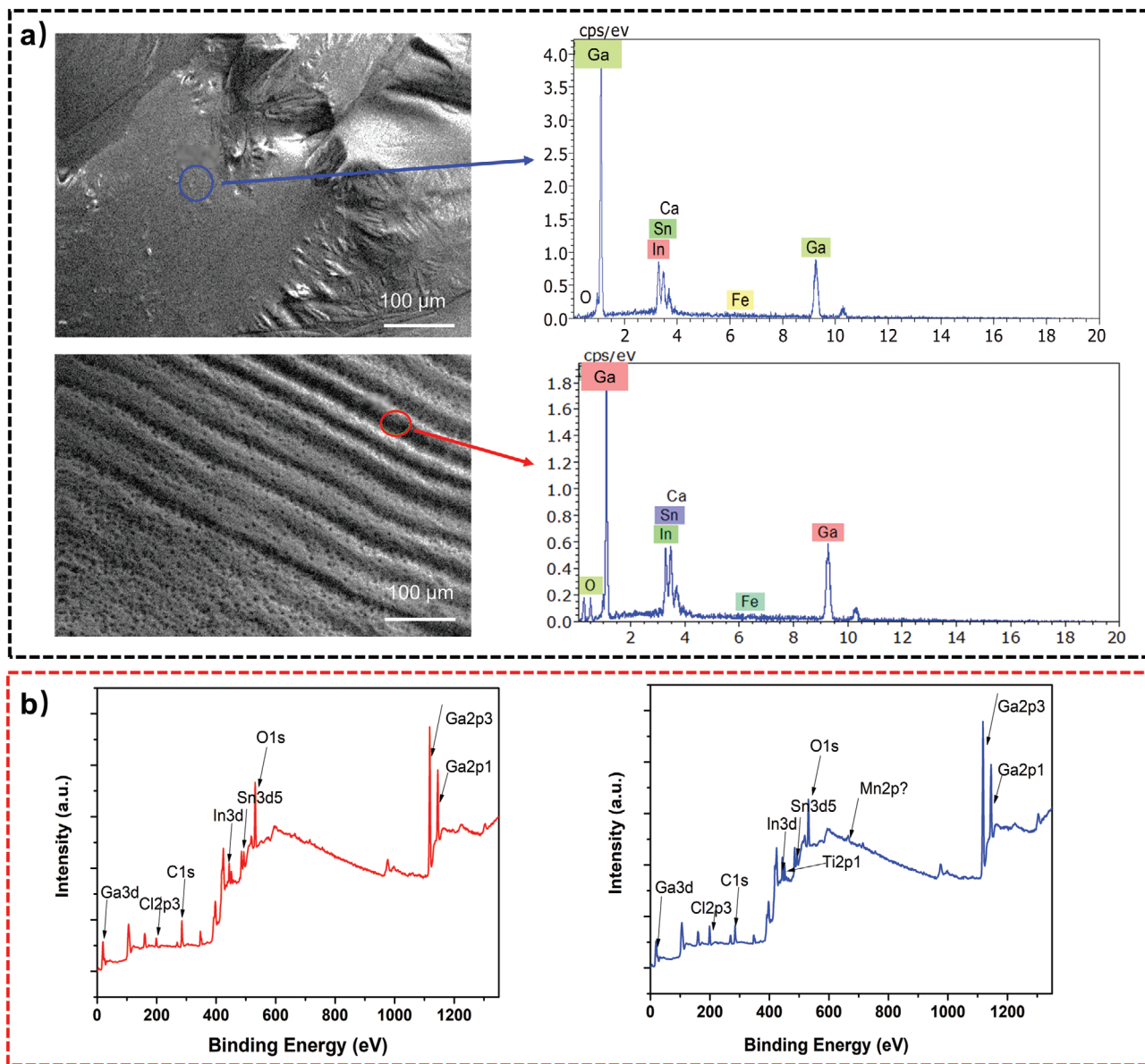


Figure 6. a) SEM and EDS of LM with normal oxide layer (above) and black oxide layer (bottom). b) XPS of GaInSn with normal oxide layer (left) and black oxide layer (right).

In 21.5%, Sn 10% by mass). The GaInSn alloy was prepared from gallium, indium, and tin with purity of 99.99%. These raw materials with mass ratios of 68.5:21.5:10 were added into a beaker and were heated to 100 °C. A magnetic stirrer was used to stir the mixture uniformly after the metals had all melted. The alloy was used in the subsequent experiments. Gelatin and calcium chloride were purchased from Sigma-Aldrich. Briefly, the gelatin (5%, w/w) was added into different calcium chloride (CaCl_2) concentration solutions (20, 40, 60, 80 mM). Then stirring until completely dissolved at around 50 °C. Finally, cooling down to make molecule crosslinking and forming the appropriate gelatin hydrogel. Deionized water (Milli-Q System, Millipore, USA) was used in all experiments.

Printing Method: The printing system was fabricated by three parts, including 3D printing system, voltage stabilizer, and injection pump. The GaInSn alloy was extruded using a syringe. And the pattern was controlled by the 3D printer through PLT file. Voltage stabilizer was used to control alloy forming.

Characterization Methods: The rheological behavior of gelatin hydrogel was detected by the rheological meter (RHEO3000). The prepared liquid metal wire was dried at room temperature for 24 h, and then its morphology and elemental analysis were examined using a field-emission SEM (ZEISS Ultra 55) and EDS. An ESCALAB 250 XPS (Thermo Fisher Scientific Company, USA) was used to test the chemical compositions of LM prepared by electronic printing. And digital multimeter (Victor VC890c) with the minimum accuracy (0.1 Ω) was used to detect the resistance of printed LM. Differential scanning calorimeter (DSC, Mettler DSC III) was used to measure the freezing and melting temperature points of different liquid metals, with initial temperature 20 °C and rising/cooling rate 10 °C min⁻¹.

Supporting Information

Supporting Information is available from the Wiley Online Library or from the author.

Acknowledgements

This work is supported by the National Natural Science Foundation of China (Grant No. 81801794), Beijing Natural Science Foundation (Grand No. 7202104) and the fund of the State Key Laboratory of Solidification Processing in NWPU (Grant No. SKLSP202111).

Conflict of Interest

The authors declare no conflict of interest.

Data Availability Statement

The data that supports the findings of this study are available in the supplementary material of this article.

Keywords

3D printing, gallium-based alloy, low melting point metal, wire-forming

Received: February 25, 2021

Revised: June 2, 2021

Published online:

- [1] H. A. Balogun, R. Sulaiman, S. S. Marzouk, A. Giwa, S. W. Hasan, *J. Water Process. Eng.* **2019**, *31*, 100786.
- [2] C. Sun, S. Liu, X. Shi, C. Lai, J. Liang, Y. Chen, *Chem. Eng. J.* **2020**, *381*, 122641.
- [3] C. Xu, G. Dai, Y. Hong, *Acta Biomater.* **2019**, *95*, 50.
- [4] M. Xie, Q. Gao, J. Qiu, J. Fu, Z. Chen, Y. He, *Biomater. Sci.* **2020**, *8*, 109.
- [5] M. Liao, H. Liao, J. Ye, P. Wan, L. Zhang, *ACS Appl. Mater. Interfaces* **2019**, *11*, 47358.
- [6] H. Gao, J. Kelly, X. Zhang, Z. Wang, *IEICE Electronics Express* **2019**, *16*, 20190485.
- [7] X. Wang, R. Guo, J. Liu, *Adv. Mater. Technol.* **2018**, *4*, 1800549.
- [8] Y. Yu, J. Zhang, J. Liu, *PLoS One* **2013**, *8*, e58771.
- [9] J. Ni, H. Ling, S. Zhang, Z. Wang, Z. Peng, C. Benyshek, R. Zan, A. K. Miri, Z. Li, X. Zhang, J. Lee, K. J. Lee, H. J. Kim, P. Tebon, T. Hoffman, M. R. Dokmeci, N. Ashammakhi, X. Li, A. Khademhosseini, *Mater. Today Bio* **2019**, *3*, 100024.
- [10] K. Kim, J. Choi, Y. Jeong, I. Cho, M. Kim, S. Kim, Y. Oh, I. Park, *Adv. Healthcare Mater.* **2019**, *8*, 1900978.
- [11] L. Fan, M. Duan, Z. Xie, K. Pan, X. Wang, X. Sun, Q. Wang, W. Rao, J. Liu, *Small* **2019**, *16*, 1903421.
- [12] C. Buchanan, L. Gardner, *Eng. Struct.* **2019**, *180*, 332.
- [13] L. Wang, J. Liu, *Front. Mater.* **2019**, *6*, 303.
- [14] V. T. Bharambe, J. Ma, M. D. Dickey, J. J. Adams, *IEEE Access* **2019**, *7*, 134245.
- [15] X. He, J. Wu, T. Hu, S. Xuan, X. Gong, *Microfluid. Nanofluid.* **2020**, *24*, 30.
- [16] W. Xinpeng, G. Jiarui, H. Liang, *Sci. China: Technol. Sci.* **2021**, *64*, 681.
- [17] Z. Yu, F. F. Yun, X. Wang, *Mater. Horiz.* **2018**, *5*, 36.
- [18] Y. Lu, Q. Hu, Y. Lin, D. B. Pacardo, C. Wang, W. Sun, F. S. Ligler, M. D. Dickey, Z. Gu, *Nat. Commun.* **2015**, *6*, 10066.
- [19] U. Daalkhaijav, O. D. Yirmibesoglu, S. Walker, Y. Mengüç, *Adv. Mater. Technol.* **2018**, *3*, 1700351.
- [20] B. Yuan, C. Zhao, X. Sun, J. Liu, *Adv. Funct. Mater.* **2020**, *30*, 1910709.
- [21] X. Wang, H. Gu, Z. Wang, L. Jiang, Y. He, Z. Yu, F. F. Yun, *Natl. Sci. Rev.* **2020**, *7*, 366.
- [22] C. Ladd, J. H. So, J. Muth, M. D. Dickey, *Adv. Mater.* **2013**, *25*, 5081.
- [23] J. W. Boley, E. L. White, G. T. C. Chiu, R. K. Kramer, *Adv. Funct. Mater.* **2014**, *24*, 3501.
- [24] M. D. Dickey, *Adv. Mater.* **2017**, *29*, 1606425.
- [25] Y. Yu, F. Liu, R. Zhang, J. Liu, *Adv. Mater. Technol.* **2017**, *2*, 1700173.
- [26] M. R. Khan, C. B. Eaker, E. F. Bowden, M. D. Dickey, *Proc. Natl. Acad. Sci. USA* **2014**, *111*, 14047.
- [27] J. Han, J. Tang, S. A. Idrus-Saidi, M. J. Christoe, A. P. O'Mullane, K. Kalantar-Zadeh, *ACS Appl. Mater. Interfaces* **2020**, *12*, 31010.
- [28] M. Mayyas, M. Mousavi, M. B. Ghasemian, R. Abbasi, H. Li, M. J. Christoe, J. Han, Y. Wang, C. Zhang, M. A. Rahim, J. Tang, J. Yang, D. Esrafilzadeh, R. Jalili, F. M. Allioux, A. P. O'Mullane, K. Kalantar-Zadeh, *ACS Nano* **2020**, *14*, 14070.
- [29] X. Wang, X. Liu, P. Bi, Y. Zhang, L. Li, J. Guo, Y. Zhang, X. Niu, Y. Wang, L. Hu, Y. Fan, *ACS Appl. Mater. Interfaces* **2020**, *12*, 53966.
- [30] Q. Wang, Y. Yu, J. Liu, *Adv. Eng. Mater.* **2018**, *20*, 1700781.
- [31] L. Zhu, B. Wang, S. Handschuh-Wang, X. Zhou, *Small* **2020**, *16*, 1903841.
- [32] J. Tang, S. Lambie, N. Meftahi, A. J. Christofferson, J. Yang, M. B. Ghasemian, J. Han, F.-M. Allioux, M. A. Rahim, M. Mayyas, T. Daeneke, C. F. McConville, K. G. Steenbergen, R. B. Kaner, S. P. Russo, N. Gaston, K. Kalantar-Zadeh, *Nat. Nanotechnol.* **2021**, *16*, 431.
- [33] L. Wang, J. Liu, *Sci. China: Technol. Sci.* **2014**, *57*, 1721.
- [34] Y. Yu, F. Liu, J. Liu, *Rapid Prototyping J.* **2017**, *23*, 642.
- [35] M. Song, K. Kartawira, K. D. Hillaire, C. Li, C. B. Eaker, A. Kiani, K. E. Daniels, M. D. Dickey, *Proc. Natl. Acad. Sci. USA* **2020**, *117*, 19026.
- [36] T. Daeneke, K. Khoshmanesh, N. Mahmood, I. A. de Castro, D. Esrafilzadeh, S. J. Barrow, M. D. Dickeyb, K. Kalantar-zadeh, *Chem. Soc. Rev.* **2018**, *47*, 4073.
- [37] M. Woo, *Proc. Natl. Acad. Sci. USA* **2020**, *117*, 5088.
- [38] H. Wang, B. Yuan, S. Liang, R. Guo, W. Rao, X. Wang, H. Chang, Y. Ding, J. Liu, L. Wang, *Mater. Horiz.* **2018**, *5*, 222.
- [39] J. Zhang, L. Sheng, J. Liu, *Sci. Rep.* **2014**, *4*, 7116.
- [40] S. Handschuh-Wang, Y. Chen, L. Zhu, X. Zhou, *ChemPhysChem* **2018**, *19*, 1584.